Warm and cool nearshore plumes connecting the surf zone to the inner shelf

M. Moulton[1,2], C. C. Chickadel[1], and J. Thomson[1]

[1]Applied Physics Laboratory, University of Washington, Seattle, WA, USA
[2]Climate & Global Dynamics Laboratory, National Center for Atmospheric Research, Boulder, CO, USA

Key Points:

- Airborne infrared imagery on the CA coast shows cool and warm plumes driven by rip currents that connect the surf zone to the inner shelf
- The surface cross-shore extent of warm plumes is about one surfzone width larger than that of cool plumes in observations and simulations
- Modeled cool nearshore plumes entering a stratified shelf subduct, whereas warm plumes extend offshore in a near-surface layer

Corresponding author: Melissa Moulton, mmoulton@apl.uw.edu

Abstract

Cross-shore transport of larvae, pollutants, and sediment between the surf zone and the inner shelf is important for coastal water quality and ecosystems. Rip currents are known to be a dominant pathway for exchange, but the effects of horizontal temperature and salinity gradients are not well understood. Airborne visible and infrared imaging performed on the California coast shows warm and cool plumes driven by rip currents in the surf zone and extending onto the shelf, with temperature differences of approximately 1°C. The airborne imagery and modeled temperatures and tracers indicate that warm plumes exhibit more lateral spreading and transport material in a buoyant near-surface layer, whereas cool plumes move offshore in a subsurface layer. The average cross-shore extent of warm plumes at the surface is approximately one surfzone width larger than for cool plumes. Future work may explore the sensitivity of nearshore plumes to density patterns, wave forcing, and bathymetry.

Plain Language Summary

Waves and currents in the coastal ocean move plankton, pollutants, nutrients, and sediment between the beach and deeper waters, impacting ecosystems and water quality. Rip currents, strong narrow seaward currents caused by breaking waves, provide a conduit for larvae to move offshore and also carry pollutants away from the beach. One common type of rip current formed in channels interrupting sandbars can sometimes be observed as a plume of brown sediment-laden water moving offshore. Previous studies of this rip-current type have assumed that the movement of material by these currents is not affected by differences in the water density (temperature and salinity) between shallower and deeper water. However, thermal (infrared) images taken from an aircraft on the coast of California show that the wave-breaking region near the beach is often significantly cooler or warmer than the ocean immediately offshore. Rip currents in these images and in numerical simulations appear either as warm plumes, which carry material further offshore and are concentrated at the water surface, or cool plumes, which move material offshore under the surface. The results show that differences in water temperature from the beach to deeper water impact how rip currents move material in the coastal ocean.

1 Introduction

Transport pathways of pollutants, nutrients, sediment, larvae, and heat in the transition from the shoreline to the shelf are important for coastal ecosystem health and water quality (Grant et al., 2005; Boehm et al., 2017). Bathymetric rip currents, strong seaward currents generated by wave breaking on channels and other alongshore-varying bathymetry in the surf zone (Bowen, 1969), are a dominant driver of cross-shore exchange in this region (Morgan et al., 2018). Signatures of rip-current circulation patterns can be observed extending onto the shelf, sometimes in the form of a turbid plume with elevated surface roughness (Smith & Largier, 1995; Haller et al., 2014) (Figure 1a). While the dynamics of bathymetric rip currents in the well-mixed surf zone are well understood and have been the subject of many observational and modeling studies (Dalrymple et al., 2011; Castelle et al., 2016), few studies have measured or assessed the importance of horizontal temperature and salinity variations as these currents evolve on the shelf.

Several field studies have observed that the surf zone may have a different temperature or salinity than water on the adjacent shelf, which is often stratified (Smith & Largier, 1995; Marmorino et al., 2013; Kastner et al., 2019; Hally-Rosendahl et al., 2014; Grimes, Feddersen, Giddings, & Pawlak, 2020). This may result in rip-current-driven nearshore plumes with a warm or cool temperature signature (Figure 1b,c). While temperature effects have not yet been investigated in persistent bathymetric rip current systems, the interaction of shelf stratification with stochastic surfzone eddy ejections, also known as transient rip currents, has been investigated in modeling and observational studies (Hally-Rosendahl et al., 2014; Suanda & Feddersen, 2015; Grimes, Feddersen, Giddings, & Pawlak, 2020; Grimes, Feddersen, & Kumar, 2020). Models have shown that, under stratified shelf conditions, transient rip currents eject eddies that move material several surfzone widths offshore in a subducted layer, thereby altering shelf stratification and circulation (Kumar & Feddersen, 2017a, 2017b, 2017c). However, the importance of horizontal density gradients between the surf zone and the inner shelf has not previously been investigated in detail using observations or models.

Bathymetric rip currents that form in channels at fixed locations (Dalrymple et al., 2011; Castelle et al., 2016) result in persistent plumes, differing from transient rip current processes that episodically eject material at changing locations. Fixed bathymetric rip current plumes may resemble other previously studied geophysical plume systems, including small river plumes (Cole & Hetland, 2016) when the surf zone is buoyant relative to water on the shelf, or subduction at ocean fronts (Rudnick & Luyten, 1996) when the surf zone is dense relative to surface waters on the shelf, but additional observations and analyses are needed to understand the dynamics of nearshore plumes.

In this paper, airborne infrared and visible observations on the Central California coast and idealized model simulations with an initially warm or cool surf zone are analyzed to investigate behaviors of plumes generated by rip currents in the presence of horizontal temperature gradients. In Section 2, observational and modeling methods are described. Sections 3 and 4 describe and discuss the results, and conclusions are presented in Section 5.

2 Methods

2.1 Airborne observations

Airborne remote sensing observations were collected on the Central CA coast near Point Sal in Sept–Oct 2017 as part of the Office of Naval Research Inner Shelf Departmental Research Initiative (Kumar et al., 2020). Observations spanned 60-km of coastline with multiple headlands, channeled nearshore morphology, and little freshwater influence.

Flights with visible and thermal infrared cameras (DRS uc640 microbolometers, sensitive to 7–14 μm) were performed on 13 days during daylight hours along several 15-km segments of coastline. Each 15-km swath, imaging a 2.5 km region from the shoreline to approximately 20-m depth, was completed in 10 minutes. For the flight altitude of 3000 ft, the resolution of the visible and infrared imagery is approximately 0.5 m and 2 m, respectively. The two infrared cameras and one visible camera were mounted obliquely to increase the image footprint. Images were rectified to geographic coordinates using onboard GPS and IMU data and intrinsic camera calibrations.

Temperature is estimated from the infrared imagery using a linear calibration with irradiance derived for the sea-surface temperature band, yielding a temperature resolution of 0.03K (Torgersen et al., 2001; Nugent et al., 2009; Forney et al., 2013). Signals are predominantly (>90%) emitted at the infrared airborne incidence angles of 20–80°. The optical depth in water for thermal longwave infrared sensors is 10–20 microns, and thus the temperature estimates include near-surface ocean temperature variability, including the formation and disruption of the millimeter-scale skin-layer, which can be O(0.1°C) cooler than the bulk water below when there is an outward heat flux from the ocean (Saunders, 1967). In addition, diurnal warm layers O(1° C) resulting from solar heating lead to temperature stratification in the upper several-meters of the water column (Fairall et al., 1996). Here, horizontal differences in skin-temperature effects are assumed to be small, and remotely sensed temperatures gradients are attributed primarily to differences in near-surface water-column temperatures.

A subset of the airborne infrared and visible observations were analyzed quantitatively to identify plume type (warm or cool), surface cross-shore extent (white arrows in Figure 1b,c), and surfzone width (arrow in Figure 1a). On the days these quantities were estimated, Sept. 16 and Oct. 11, 2017, which were representative of overall experiment conditions, 97 cool plumes and 92 warm plumes were identified. Manual identification of plumes and their surface extents was used after limited success identifying plumes with a more automated approach using temperature contours. The surface cross-shore extent of each plume was defined as the cross-shore distance between the shoreline and the manually identified location of the strong temperature front at the plume edge. The plume extents were normalized by a set of temporally and spatially varying surfzone widths near each plume, estimated in visible imagery as the cross-shore extent of the bright breaking region. The estimates of surfzone width varied from $L_{sz} = 70-103m$ on Sept. 16 and from $L_{sz} = 96-145m$ on Oct. 11. Bulk plume extent statistics results varied by less than 20% when normalizing by an average versus varying surfzone width.

2.2 Idealized modeling of nearshore plumes

Nearshore plumes resulting from bathymetric rip currents are simulated with the Coupled Ocean Wave Atmosphere Sediment Transport modeling system (COAWST), a fully three-dimensional coupled wave-current-sediment transport model that has skill simulating surfzone and inner shelf observations (Warner et al., 2008, 2010; Kumar et al., 2011, 2012, 2015, 2016; Olabarrieta et al., 2014). COAWST couples the ocean circulation model Regional Ocean Modeling System (ROMS) (Haidvogel et al., 2008) with the spectral wave model Simulating WAves Nearshore (SWAN) (Booij et al., 1996), and includes ocean surface and bottom stresses and surface wave transformation (shoaling, refraction on bathymetry and mean currents, depth-limited breaking, and energy loss due to bottom friction). Processes not included in COAWST, including infragravity variability, short-crested wave breaking, and transient rip currents are expected to drive higher-frequency plume variability that are beyond the focus of this study.

The idealized model domain extends from the shoreline to 23.5-m depth and spans 3 km alongshore with 2-m horizontal resolution and 10 uniformly spaced vertical terrain-following layers (subset of domain shown in Figure 2). The ocean and wave model timestep of 0.5 s and wave-current coupling interval of 15 s were selected for model stability and to resolve timescales of plume evolution. The model is run for 2 hours to simulate the initial plume evolution. The model eddy viscosity is set to 0.2 m^2/s, similar to previous studies (Kumar et al., 2012). To generate bathymetric rip currents that result in nearshore plumes, an idealized wave spectrum similar to nearby observations (JONSWAP spectrum with significant wave height = 1 m, directional spread = 36°, wave period = 7 s, $\gamma_J = 1.0$) is specified at the offshore boundary and waves are incident on a synthetic barred beach profile interrupted by channels (Figure 2). Wave breaking on the channeled bathymetry results in alongshore gradients in wave breaking and setup, driving a bathymetric rip current in each channel (Moulton et al., 2017), with speeds up to 1 m/s. The beach slope (0.025 near shore, concave decreasing slope towards offshore boundary), bar geometry (∼60-m wide, ∼0.5 m depth at crest), and channel spacing (200 m) and width (40 m) are within the range of observed morphology at the site. Wave and ocean model parameters not described here are the same as used in a previous study of bathymetric rip currents by Moulton et al. (2017).

To simulate a warm or cool surf zone, an initial linear horizontal temperature gradient is applied ($|\Delta T| = 1$°C, as a smooth cross-shore ramp with width ∼30-m), with linear vertical stratification on the shelf ($dT/dz = 0.4°C/m$) based on observed conditions (Figure 2b,c). A simulation with uniform density also is performed (not shown). Results from simulations with different channel spacing (500 m), initial temperature difference (0.5°C, 2°C), and incident wave height (0.5 m and 0.75 m), period (10 s), and spread (20°) are qualitatively similar and sensitivity to these parameters is not explored here. In cases run with the same initial temperature distributions and no wave forcing (not shown), plumes do not form, and the horizontal temperature gradients relax slowly. To track water associated with the surfzone-originating plumes, tracer is released continuously near-bed in an alongshore strip in the surf zone (arrows in Figure 2b,c), and is normalized at each time by the total tracer to estimate a fractional tracer concentration, similar to previous studies (Kumar & Feddersen, 2017c; Grimes, Feddersen, & Kumar, 2020).

Model plume surface extents were estimated using the same method as for the observations, by computing the cross-shore distance between a manually identified plume front, consistent with the location of the strongest surface temperature gradient, and the shoreline. Model plume lengthscales are normalized by the model surfzone width, defined here as the position where the significant wave height begins decreasing in the region away from channels, here approximately L_{sz} ≈80 m for 1-m wave height (decreasing to 74 m for 0.75-m waves and 68 m for 0.5-m waves). This location, where depth-limited wave dissipation increases strongly onshore, is expected to be reasonably consistent with the surfzone width identified based on bright foam in visible imagery. The results are not sensitive to the estimate of model surfzone width, which varies by O(20%) using other commonly used definitions. The results also are not sensitive to using a constant surfzone width rather than a wave-height dependent width; bulk plume distribution statistics varied by less than 10%. Model results are analyzed at several multiples of an approximate surfzone flushing timescale, after which the system may have less dependence on the surfzone temperature initial condition. For the wave and bathymetric conditions shown here, an expected timescale for bathymetric rip currents to flush the surfzone volume is O(15 min), estimated as the surfzone volume divided by the rip current volume flux per unit alongshore width of the domain at the surfzone edge.

3 Results

3.1 Observed plume statistics

Signatures of rip-current plumes are ubiquitous in the airborne infrared dataset, appearing in the majority of swaths, with $|\Delta T|$ $0.5-2°C$ (Figure 1). The plume locations often are fixed in space over hours to days, consistent with bathymetric rip currents formed in channels. Visible airborne imagery included bright and dark signatures of channeled surfzone morphology, and radar-derived bathymetry estimates also indicated the presence of channels where plumes were observed (Holman & Haller, 2013; O'Dea et al., In Revision). More transient features with smaller temperature signals and shorter spatial scales, possibly resulting from surfzone eddy ejections, also were observed but are not studied here. Visible signatures of the plumes (Figure 1a) were typical of expected signatures of rip currents, including sediment-laden water and micro-breaking at the plume edges. The observed plumes often were cold relative to water on the shelf, while warm plumes were observed less frequently, with temperature differences up to 1°C for both cool and warm plumes.

Plume presence varied along the complex coastline, possibly as a function of incident wave energy and direction, with some sections of coastline experiencing frequent strong plume activity, and other regions with few or no observed plumes. A temporal pattern was observed during the experiment, with cool plumes more likely to occur in the morning, and warm plumes occurring in the afternoon following peak solar heating, consistent with previous studies of stochastic eddy ejections (Hally-Rosendahl et al., 2014; Grimes, Feddersen, Giddings, & Pawlak, 2020). At some times, both cold and warm plumes were present on different parts of the coastline. Changes in plume activity and temperature with tidal elevation were not evident, however the sensitivity of plumes to water levels and other conditions was not investigated in detail here. On days with large wind speeds and wave heights, plumes often were not observed in infrared imagery as a result of weaker temperature contrast, however plume signatures were observed under these conditions in radar imagery (not shown). During the selected experiment days analyzed here (Sept. 16 and Oct. 11, 2017), the tide range was about 1 m, wave heights ranged from 0.5-1.5 m, wave directions were primarily from the WNW ±45°, and wind speeds ranged from 1-5 m/s.

Cool and warm plumes both had a wide range of surface cross-shore extents normalized by the surfzone width, with cool plumes having a smaller average surface cross-shore extent of $\langle L_p/L_{sz}\rangle_{cool} = 1.8$ and warm plumes having a larger surface cross-shore extent of $(\langle L_p/L_{sz}\rangle_{warm} = 2.7$ (Figure 3). The median cool plume surface extent $((L_p/L_{sz})_{med,cool} = 1.7)$ also differed from the median warm plume surface extent $((L_p/L_{sz})_{med,warm} = 2.4)$ by nearly a surfzone width. The peak in the distribution of cool plumes with bins of width 0.5 was $L_p/L_{sz} \sim 1.5$ and the distribution is narrower than for warm plumes, which have a broader peak near $L_p/L_{sz} \sim 2.0 - 2.5$. The wide distributions of surface extents (Figure 3) may result partly from sampling different stages of the temporal evolution of cool and warm plumes, which formed at different times and were observed to change in shape and extent over timescales of tens of minutes to hours. Almost all warm plumes were observed to have surface cross-shore extents of near $L_p/L_{sz} = 1.5$ or greater, whereas many cool plumes were observed to have surface extents near $L_p/L_{sz} = 1.0$. Almost all observed cool plumes had surface extent less than $L_p/L_{sz} < 4.0$, whereas many warm plumes were observed to have $L_p/L_{sz} > 4.0$ and some warm plumes extended as far offshore as $L_p/L_{sz} \sim 6.0$.

3.2 Modeled plumes

Idealized model simulations of plumes originating in a cool or warm surf zone and extending onto a stratified shelf have similar surface temperature patterns to the remote sensing measurements and allow for investigation of subsurface plume behavior (Figure 1b,c, Figure 4). Initialization of the model with warm or cool surfzone water in otherwise identical simulations leads to substantially different surface cross-shore plume extents and vertical structure, suggesting that the relative surf-shelf temperature is a strong control on observed plume behavior. Dye in simulations with neutral-density (not shown) and the same wave forcing and bathymetry indicates that the surface cross-shore extent of neutral-density plumes is typically between that of warm and cool plumes, and that the neutral-density plumes show little vertical structure (tracers are well mixed through the water column).

As modeled rip currents eject surfzone water onto the shelf, the surface temperature and dye signatures of warm plumes extend further offshore than cool plumes and both have complex patterns. Similar to field observations (Figure 1b,c), the alongshore surface structure of cool and warm plumes differed significantly, with warm plumes exhibiting more lateral spreading and more rounded patterns, and cool plumes having narrower alongshore scales and more complex structure at the plume edges (Figure 4a,b). Both warm and cool plumes contain filaments of cooler or warmer water. At time t=45 min, the surface cross-shore extent of modeled cool plumes is approximately $(L_p/L_{sz})_{cool} \approx 1.8 - 3$, whereas for warm plumes $(L_p/L_{sz})_{cool} \approx 3.8 - 4$ (Figure 4a,b). The modeled warm plumes extend approximately one surfzone width farther offshore at this time, similar to bulk results from field observations sampling temporally complex plume evolution (Figure 3).

To simulate variability in temporal sampling and conditions similar to the field sampling, four additional simulations were analyzed for both cool and warm plumes, two with different initial $|\Delta T|$ (0.5°C, 2°C) and two with different incident wave heights (0.5 m and 0.75 m), resulting in a suite of five simulations each for cool and warm plumes. Each of these simulations was analyzed for plume surface cross-shore extent near the five channel locations at four randomly selected times (using model output at 5-min intervals from

5–60 min), yielding estimates for 100 cool plumes and 100 warm plumes. Results are not sensitive to removing half of the randomly sampled times. The resulting distributions of cool and warm plume surface extents (Figure 4c,d) had average surface extents of $\langle L_p/L_{sz}\rangle_{cool} = 2.4$ and $\langle L_p/L_{sz}\rangle_{warm} = 3.6$; warm plumes extended on average approximately one surfzone width further offshore than cool plumes, similar to the observations (Figure 3). Median plume surface extents are similar to the average extents. The modeled distributions have larger mean and median values than the observations, which may result from different sampling of conditions and times. Like the observations, cool plumes had a narrower distribution of cross-shore surface extents, whereas warm plumes had a wider distribution with more plumes observed at large surface cross-shore extents.

To investigate plume vertical structure, temperature and dye transects are shown in Figure 4e-j. The dye and temperature fields were averaged over 40-m (the channel width) centered at y=200 m (the center of one of the channels). In modeled cool plumes, surfzone-released tracer subducts to a level of neutral density into the stratified shelf (Figure 4e,f,g), similar to modeled behavior of transient rip currents (Kumar & Feddersen, 2017a; Grimes, Feddersen, & Kumar, 2020). In warm plumes, buoyant surfzone water is confined to the surface, enhancing near-surface stratification (Figure 4h,i,j). Cool or warm water leaves the surf zone in a momentum-dominated jet, and subsequently lifts off and propagates slowly offshore, consistent with the transition from a jet to a gravity current. At the outer edge of the surf zone, the modeled cross-shore current speeds in the channels of approximately 0.5 m/s are similar to speeds in simulations with uniform density, and are in agreement with expected breaking-wave driven bathymetric rip current speeds (Moulton et al., 2017). The plume liftoff location, approximately where temperature contours intersect the bed, is consistent at each time with the location where a baroclinic Froude number reaches unity (Figure 4e-j, triangles). This Froude number is defined for nearshore plumes as $Fr_p = U_p/\sqrt{g'h}$, where U_p is the depth-averaged plume velocity and $\sqrt{g'h}$ is a baroclinic phase speed, a function of the reduced gravity g' (here set as a constant value based on the initial $|\Delta T|$) and the water depth h. The plume velocity U_p and the water depth h both vary in the cross-shore, and are estimated as averages over 40-m alongshore distance. For the suite of model cases, comparison of dye fields for warm and cool plumes indicates that for the same $|\Delta T|$, the warm-plume surface propagation speeds and surface cross-shore extents are of the same order of magnitude but somewhat greater than the cool-plume subsurface speeds and extents (e.g., Figure 4g,j).

Analysis of the temporal evolution of the mean modeled plume surface extents indicates that modeled cool plumes stabilized to an approximately constant value, whereas the warm plume extents increased in time (Figure 4k,l). The existence of an equilibrium position for the cool plume subduction front is consistent with the smaller mean lengthscale and narrower distribution of observed and modeled surface plume extents. Cool plumes with larger ΔT has a slightly smaller surface extents (Figure 4k, symbols), possibly as a result of an earlier transition to buoyancy dominated current. The larger standard deviation of the cool plumes extents at each time may reflect sensitivity of the subduction front to instabilities and adjacent plumes (Figure 4a,k). Warm plumes propagated offshore at the surface continuously, at a rate much slower than the rip-current jet speeds of 0.4-0.5 m/s and within the range of expected gravity current speeds from 0.05-0.15 m/s (Figure 4l, slopes of dotted and dashed lines, plotted for L_{sz}=80 m). This range of speeds was computed as the range of $\sqrt{(g'h)}$ for $0.5 < \Delta T < 2°$C and plume height $2 < h < 5m$. The continuous surface propagation of warm plumes is consistent with the larger mean lengthscale and broader distribution of the observed and modeled surface plume extents sampled at a range of times. At each time, the surface extent of warm plumes was slightly larger for larger ΔT, and the warm plume speeds decreased with time and increasing cross-shore distance (Figure 4l, symbols).

At later times in the simulation (not shown), warm water initialized in the surf zone flushes out and the ejected warm water continues to laterally spread and mix, with a decaying plume temperature signature. In contrast, cool plumes continue to persist beyond several surfzone flushing timescales, possibly as a result of continued entrainment of cool water into the surf zone. Similar to earlier times in the simulation, the persistent cool plumes have a relatively fixed cross-shore extent at the surface, the location where cool water subducts, and an increasing subsurface dye extent as the cool gravity current continues to propagate offshore.

4 Discussion

The observed spatial gradients in temperature between the surf zone and inner shelf may occur as a result of variations in water depth, solar heating, wave dissipation, and other processes. If both the shelf and surf zone are well mixed, the shallower surf zone may heat and cool more quickly in the presence of a spatially uniform diurnally varying surface heat flux, contributing to the observed occurrence of warm plumes following periods of strong heating. This spatial gradient in diurnal heating also leads to a diurnally reversing horizontal temperature gradient (Ulloa et al., 2018) driving a net two-layer cross-shore circulation that is expected to be small relative to rip-current-driven transport (Grimes, Feddersen, & Kumar, 2020). In contrast, under weak mixing conditions (e.g., low winds), a diurnal warm layer (Price et al., 1986) may form on the shelf, leading to warmer near-surface temperatures offshore of the surf zone during strong solar heating.

Other contributors to horizontal temperature gradients include spatial variations in albedo resulting from bright wave-breaking-generated foam (Sinnett & Feddersen, 2014), elevated turbidity from suspended sediment or algae (Fogarty et al., 2018), transfer of heat stored in the sediments of the intertidal beach (Rinehimer & Thomson, 2014), and heating due to wave dissipation (Sinnett & Feddersen, 2014). In addition, wind-driven flows, regional coastal circulation patterns, and propagating fronts and internal waves may drive or modulate horizontal density gradients in this region (Washburn et al., 2011; Sinnett et al., 2018; McSweeney et al., 2020; Feddersen et al., 2020). Prior results suggest these processes may drive the observed horizontal surface temperature gradients of O(1 °C) with variability on diurnal, synoptic, and seasonal timescales, however, the temporal variation and relative importance of these processes is not known. In addition, while the results suggest the dominant plume behaviors are explained well by a simple model with an initial horizontal temperature gradient, aspects of the nearshore plume behavior may vary as a result of interaction with shelf processes including internal waves, fronts, and adjacent plumes.

Horizontal differences in near-surface mixing and resulting disruption of cool skins or diurnal warm layers (Saunders, 1967; Fairall et al., 1996) may contribute to the observed temperature differences between the surf zone and the shelf. The results here are not expected to be affected by O(0.1°C) differences in cool-skin formation that may occur as a result of differences in near-surface mixing between the surf zone and the shelf. Diurnal warm layer formation O(1°C) enhances near-surface stratification and may affect interpretation of the remote sensing measurements and the vertical structure of plumes. Future work incorporating models of the upper ocean temperature profile behavior (Fairall et al., 2003) would allow for more detailed understanding of relationships between the airborne skin temperature measurements and observed and modeled near-surface and subsurface temperature gradients.

Results shown here indicate commonalities between nearshore plumes generated by rip currents and small buoyant plumes or subducting gravity currents. Still, further study is needed to improve understanding of these features, including controls on mixing and entrainment at plume boundaries, rates of plume spreading, cross-shore exchange, and the temporal evolution of plumes at timescales from individual waves to diurnal to seasonal forcing. Further comparison of uniform and variable-density plume behavior will aid understanding of how rip-current vertical structure is modulated by density. While this analysis focused on temperature variability, the results may be applicable to salinity variations near small river mouths where freshwater transported along-coast escapes through the surf zone. The airborne images and model initial-condition experiments presented here provide insight into bulk differences between warm and cool nearshore plumes driven by rip currents.

5 Conclusions

Airborne infrared imagery on the California coast shows cool and warm plumes connecting the surf zone to the inner shelf. These plumes are driven by rip currents in the surf zone that transport water offshore in a narrow jet that transitions to a buoyancy-controlled plume. In both observations and simulations, the surface cross-shore extent of warm plumes is about one surfzone width larger than that of cool plumes. Modeled cool nearshore plumes entering a stratified shelf subduct to a level of neutral density, whereas warm plumes extend offshore in a near-surface layer. This work indicates that the temperature of rip-current plumes affects the horizontal and vertical structure of the exchange of tracers from the surf zone to the shelf.

Acknowledgments

Observations were collected as part of the Office of Naval Research Inner Shelf Dynamics Experiment effort to study inner shelf processes. Additional support was provided by the University of Washington Royalty Research Fund and the Office of Naval Research Young Investigator Program. Thanks to experiment participants for a team effort to collect field measurements and for providing feedback on this work. Observations are available in the Inner Shelf data repository hosted by UC San Diego Library (full dataset: https://doi.org/10.6075/J0WD3Z3Q, airborne data: https://doi.org/10.6075/J0C24TZJ) and model results and input files are available at Zenodo.org (https://doi.org/10.5281/zenodo.4272080).

References

Boehm, A. B., Ismail, N. S., Sassoubre, L. M., & Andruszkiewicz, E. A. (2017). Oceans in Peril: Grand Challenges in Applied Water Quality Research for the 21st Century. *Environmental Engineering Science*, *34*(1), 3–15. doi: 10.1089/ees.2015.0252

Booij, N., Holthuijsen, L. H., & Ris, R. C. (1996). The "SWAN" Wave Model for Shallow Water. *Coastal Engineering*, 668–676. doi: 10.9753/icce.v25.%p

Bowen, A. J. (1969). Rip currents: 1. Theoretical investigations. *Journal of Geophysical Research*, *74*(23), 5467. doi: 10.1029/JC074i023p05467

Castelle, B., Scott, T., Brander, R., & McCarroll, R. (2016). Rip Current Types, Circulation and Hazard. *Earth-Science Reviews*, *163*, 1–21. doi: 10.1016/j.earscirev.2016.09.008

Cole, K. L., & Hetland, R. D. (2016). The effects of rotation and river discharge on net mixing in small mouth Kelvin number plumes. *Journal of Physical Oceanography*, *46*(2010), 1421–1436. doi: 10.1175/JPO-D-13-0271.1

Dalrymple, R. a., MacMahan, J. H., Reniers, A. J. H. M., & Nelko, V. (2011, jan). Rip Currents. *Annual Review of Fluid Mechanics*, *43*(1), 551–581. doi: 10.1146/annurev-fluid-122109-160733

Fairall, C. W., Bradley, E. F., Godfrey, J. S., Wick, G. A., Edson, J. B., & Young, G. S. (1996). Cool-skin and warm-layer effects on sea surface temperature. *Journal of Geophysical Research: Oceans*, *101*(C1), 1295–1308. doi: 10.1029/95JC03190

Fairall, C. W., Bradley, E. F., Hare, J. E., Grachev, A. A., & Edson, J. B. (2003). Bulk parameterization of air-sea fluxes: Updates and verification for the COARE algorithm. *Journal of Climate*, *16*(4), 571–591. doi: 10.1175/1520-0442(2003)016⟨0571:BPOASF⟩2.0.CO;2

Feddersen, F., MacMahan, J. H., Freismuth, T. M., Gough, M. K., & Kovatch, M. (2020). Inner-Shelf Vertical and Alongshore temperature Variability in the Subtidal, Diurnal, and Semidiurnal Bands Along the central California coastline with headlands. *Journal of Geophysical Research: Oceans*, *125*(3), 1–24. doi: 10.1029/2019jc015347

Fogarty, M. C., Fewings, M. R., Paget, A. C., & Dierssen, H. M. (2018). The Influence of a Sandy Substrate, Seagrass, or Highly Turbid Water on Albedo and Surface Heat Flux. *Journal of Geophysical Research: Oceans*, *123*, 53–73. doi: 10.1002/2017JC013378

Forney, W. M., Soulard, C. E., & Chickadel, C. C. (2013). Salmonids, Stream Temperatures, and Solar Loading—Modeling the Shade Provided to the Klamath River by Vegetation and Geomorphology. *USGS Scientific Investigations Report 2013-5022*.

Grant, S. B., Kim, J. H., Jones, B. H., Jenkins, S. A., Wasyl, J., & Cudaback, C. (2005). Surf zone entrainment, along-shore transport, and human health implications of pollution from tidal outlets. *Journal of Geophysical Research C: Oceans*, *110*(10), 1–20. doi: 10.1029/2004JC002401

Grimes, D. J., Feddersen, F., Giddings, S. N., & Pawlak, G. (2020). Cross-shore deformation of a surfzone released dye plume by an internal tide on the inner-shelf. *Journal of Physical Oceanography*, *50*(1), 35–54. doi: 10.1175/JPO-D-19-0046.1

Grimes, D. J., Feddersen, F., & Kumar, N. (2020). Tracer Exchange Across the Stratified Inner-Shelf Driven by Transient Rip-Currents and Diurnal Surface Heat Fluxes. *Geophysical Research Letters*, *47*(10), 1–12. doi: 10.1029/2019GL086501

Haidvogel, D. B., Arango, H., Budgell, W. P., Cornuelle, B. D., Curchitser, E., Di Lorenzo, E., … Wilkin, J. L. (2008). Ocean forecasting in terrain-following coordinates: Formulation and skill assessment of the Regional Ocean Modeling System. *Journal of Computational Physics*, *227*(7), 3595–3624. doi: 10.1016/j.jcp.2007.06.016

Haller, M. C., Honegger, D. A., & Catalán, P. (2014). Rip current observations via marine radar. *Journal of Waterway, Port, Coastal, and Ocean Engineering*, *140*(April), 115–124. doi: 10.1061/(ASCE)WW.1943-5460.0000229.

Hally-Rosendahl, K., Feddersen, F., & Guza, R. T. (2014). Cross-shore tracer exchange between the surfzone and inner-shelf. *Journal of Geophysical Research: Oceans*, *119*(7), 4367–4388. doi: 10.1002/2013JC009722

Holman, R. A., & Haller, M. C. (2013, jan). Remote Sensing of the Nearshore. *Annual Review of Marine Science*, *5*(1), 95–113. Retrieved from `http://www.ncbi.nlm.nih.gov/pubmed/22809186` doi: 10.1146/annurev-marine-121211-172408

Kastner, S. E., Horner-Devine, A. R., & Thomson, J. M. (2019). A Conceptual Model of a River Plume in the Surf Zone. *Journal of Geophysical Research: Oceans*, *124*(11), 8060–8078. doi: 10.1029/2019JC015510

Kumar, N., & Feddersen, F. (2017a). The Effect of Stokes Drift and Transient Rip Currents on the Inner Shelf. Part II: With Stratification. *Journal of Physical Oceanography*, *47*(1), 243–260. doi: 10.1175/JPO-D-16-0077.1

Kumar, N., & Feddersen, F. (2017b). The Effect of Stokes Drift and Transient Rip Currents on the Inner Shelf. Part I: No Stratification. *Journal of Physical Oceanography*, *47*(1), 227–241. doi: 10.1175/JPO-D-16-0076.1

Kumar, N., & Feddersen, F. (2017c). A new offshore transport mechanism for shoreline-released tracer induced by transient rip currents and stratification. *Geophysical Research Letters*, *44*(6), 2843–2851. doi: 10.1002/2017GL072611

Kumar, N., Feddersen, F., Suanda, S., Uchiyama, Y., & McWilliams, J. (2016). Midto Inner-Shelf Coupled ROMS–SWAN Model–Data Comparison of Currents and Temperature: Diurnal and Semidiurnal Variability. *Journal of Physical Oceanography*, *46*(3), 841–862. doi: 10.1175/JPO-D-15-0103.1

Kumar, N., Feddersen, F., Uchiyama, Y., McWilliams, J. C., & O'Reilly, W. (2015). Midshelf to Surfzone Coupled ROMS–SWAN Model Data Comparison of Waves, Currents, and Temperature: Diagnosis of Subtidal Forcings and Response. *Journal of Physical Oceanography*, *45*(6), 1464–1490. doi: 10.1175/JPO-D-14-0151.1

Kumar, N., Lerczak, J. A., Xu, T., Waterhouse, A. F., Thomson, J., Terrill, E. J., ... Ahn, S. (2020). The inner-shelf dynamics experiment. *Bulletin of the American Meteorological Society*, 1 - 77. Retrieved from `https://journals.ametsoc.org/view/journals/bams/aop/BAMS-D-19-0281.1/BAMS-D-19-0281.1.xml` doi: 10.1175/BAMS-D-19-0281.1

Kumar, N., Voulgaris, G., & Warner, J. C. (2011, dec). Implementation and modification of a three-dimensional radiation stress formulation for surf zone and rip-current applications. *Coastal Engineering*, *58*(12), 1097–1117. doi: 10.1016/j.coastaleng.2011.06.009

Kumar, N., Voulgaris, G., Warner, J. C., & Olabarrieta, M. (2012). Implementation of the vortex force formalism in the coupled ocean-atmosphere-wave-sediment transport (COAWST) modeling system for inner shelf and surf zone applications. *Ocean Modelling*, *47*, 65–95. doi: 10.1016/j.ocemod.2012.01.003

Marmorino, G. O., Smith, G. B., & Miller, W. D. (2013). Infrared remote sensing of surf-zone eddies. *IEEE Journal of Selected Topics in Applied Earth Observations and Remote Sensing*, *6*(3), 1710–1718. doi: 10.1109/JSTARS.2013.2257695

McSweeney, J. M., Lerczak, J. A., Barth, J. A., Becherer, J., Colosi, J. A., Mackinnon, J. A., ... Waterhouse, A. F. (2020). Observations of shoaling nonlinear internal bores across the Central California inner shelf. *Journal of Physical Oceanography*, *50*(1), 111–132. doi: 10.1175/JPO-D-19-0125.1

Morgan, S. G., Shanks, A. L., MacMahan, J. H., Reniers, A. J., & Feddersen, F. (2018). Planktonic subsidies to surf-zone and intertidal communities. *Annual Review of Marine Science*, *10*, 345–369. doi: 10.1146/annurev-marine-010816-060514

Moulton, M., Elgar, S., Raubenheimer, B., Warner, J. C., & Kumar, N. (2017). Rip currents and alongshore flows in single channels dredged in the surf zone. *Journal of Geophysical Research: Oceans*, *122*(5), 3799–3816. doi: 10.1002/2016JC012222

Nugent, P. W., Shaw, J. A., Pust, N. J., & Piazzolla, S. (2009). Correcting calibrated infrared sky imagery for the effect of an infrared window. *Journal of Atmospheric and Oceanic Technology*, *26*(11), 2403–2412. doi: 10.1175/2009JTECHA1288.1

O'Dea, A. O., Kumar, N., & Haller, M. C. (In Revision). Simulations of the surf zone eddy field and cross-shore exchange on a non-idealized bathymetry. *Journal of Geophysical Research: Oceans*.

Olabarrieta, M., Geyer, W. R., & Kumar, N. (2014). The role of morphology and wave-current interaction at tidal inlets: An idealized modeling analysis. *Journal of Geophysical Research: Oceans*, *119*(12), 8818–8837. doi: 10.1002/2014JC010191

Price, J. F., Weller, R. A., & Pinkel, R. (1986). Diurnal Cycling: observations and models of the upper ocean response to diurnal heating, cooling, and wind mixing. *Journal of Geophysical Research: Oceans*, *91*(6), 8411–8427. doi: 10.1029/jc091ic07p08411

Rinehimer, J. P., & Thomson, J. T. (2014). Observations and modeling of heat fluxes on tidal flats. *Journal of Geophysical Research: Oceans*, *119*(1), 133–146. doi: 10.1002/2013JC009225

Rudnick, D. L., & Luyten, J. R. (1996). Intensive surveys of the Azores Front 1. Tracers and dynamics. *Journal of Geophysical Research C: Oceans*, *101*(C1), 923–939. doi: 10.1029/95JC02867

Saunders, P. M. (1967). The Temperature at the Ocean-Air Interface. *Journal of the Atmospheric Sciences*, *24*(3), 269–273. doi: 10.1175/1520-0469(1967)024⟨0269:ttatoa⟩2.0.co;2

Sinnett, G., & Feddersen, F. (2014). The surf zone heat budget: The effect of wave heating. *Geophysical Research Letters*, *41*(20), 7217–7226. doi: 10.1002/2014GL061398

Sinnett, G., Feddersen, F., Lucas, A. J., Pawlak, G., & Terrill, E. (2018). Observations of Nonlinear Internal Wave Run-Up to the Surfzone. *Journal of Physical Oceanography*, *48*(3), 531–554. doi: 10.1175/JPO-D-17-0210.1

Smith, J. A., & Largier, J. L. (1995). Observations of nearshore circulation: Rip currents. *Journal of Geophysical Research*, *100*(C6), 10967. doi: 10.1029/95JC00751

Suanda, S. H., & Feddersen, F. (2015). A self-similar scaling for cross-shelf exchange driven by transient rip currents. *Geophysical Research Letters*, *42*(13), 5427–5434. doi: 10.1002/2015GL063944

Torgersen, C. E., Faux, R. N., McIntosh, B. A., Poage, N. J., & Norton, D. J. (2001). Airborne thermal remote sensing for water temperature assessment in rivers and streams. *Remote Sensing of Environment*, *76*(3), 386–398. doi: 10.1016/S0034-4257(01)00186-9

Ulloa, H. N., Davis, K. A., Monismith, S. G., & Pawlak, G. (2018). Temporal variability in thermally driven cross-shore exchange: The role of semidiurnal tides. *Journal of Physical Oceanography*, *48*(7), 1513–1531. doi: 10.1175/JPO-D-17-0257.1

Warner, J. C., Armstrong, B., He, R., & Zambon, J. B. (2010, jan). Development of a Coupled Ocean-Atmosphere-Wave-Sediment Transport (COAWST) Modeling System. *Ocean Modelling*, *35*(3), 230–244. doi: 10.1016/j.ocemod.2010.07.010

Warner, J. C., Butman, B., & Dalyander, P. S. (2008). Storm-driven sediment transport in Massachusetts Bay. *Continental Shelf Research*, *28*(2), 257–282. doi: 10.1016/j.csr.2007.08.008

Washburn, L., Fewings, M. R., Melton, C., & Gotschalk, C. (2011). The propagating response of coastal circulation due to wind relaxations along the central California coast. *Journal of Geophysical Research: Oceans*, *116*(12), 1–16. doi: 10.1029/2011JC007502

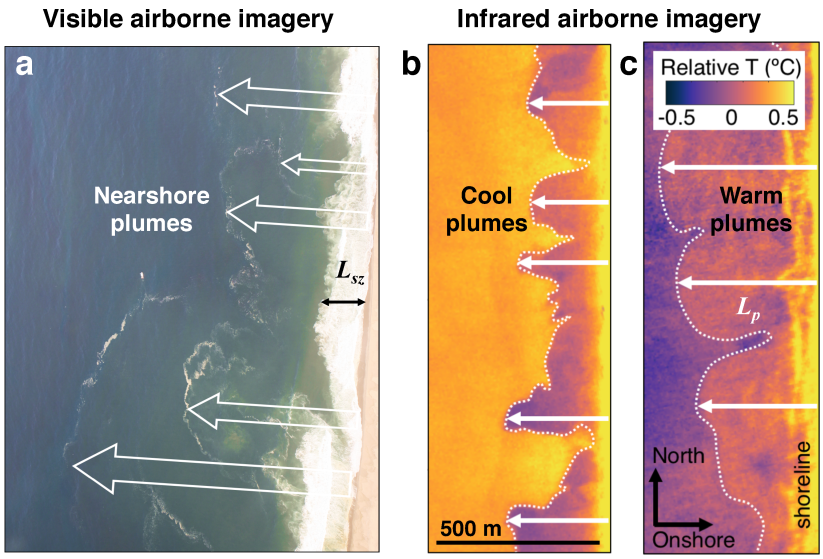

Figure 1. (a) Aerial photo of the surf zone and inner shelf along several km of coast near Pt. Sal, CA, with nearshore plumes generated by rip currents carrying sediment offshore (arrows). Airborne infrared images (georectified, scale in b) showing relative temperature (°C), with (b) cool and (c) warm plumes (dashed temperature contours: plume boundaries; arrows: plume surface cross-shore extent L_p) originating in the surf zone (width L_{sz} in a) and extending 100s of m onto the shelf.

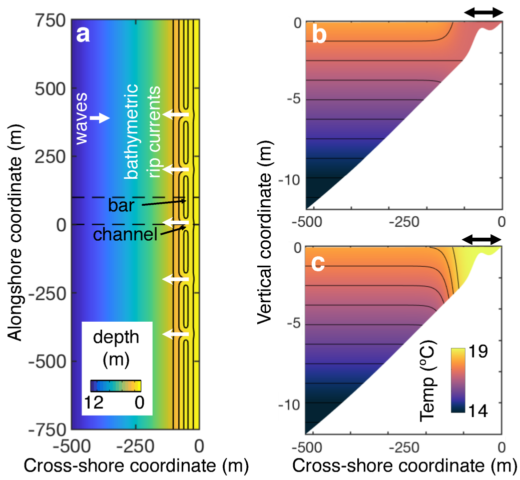

Figure 2. (a) Idealized COAWST model domain (subset of domain shown) with barred bathymetry (color contours) interrupted by a series of channels, and initial cross-shore temperature sections (color, with contours every 0.5°C) for (b) cool surf zone (c) warm surf zone ($|\Delta T|$=1°C) with linear shelf stratification. Wave breaking on the bar-channel bathymetry drives a series of bathymetric rip-current jets (a, white arrows) that emerge on the shelf as nearshore plumes, tracked here with passive tracer released in the surf zone (b,c black arrows).

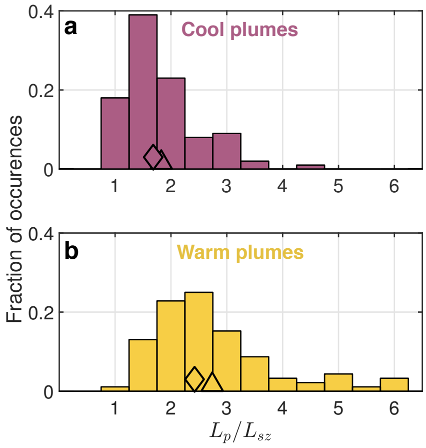

Figure 3. Histograms of the number of occurrences of (a) cool and (b) warm plumes in infrared imagery versus the ratio of the plume cross-shore surface extent (L_p, arrows in Figure 1b,c) and surfzone width (L_{sz}, Figure 1a). The average cross-shore surface extent (triangle on x axis) is $\langle L_p/L_{sz}\rangle_{cool} = 1.8$ for cool plumes and $\langle L_p/L_{sz}\rangle_{warm} = 2.7$ for warm plumes, and the median cross-shore surface extent (diamond on x axis) is $(L_p/L_{sz})_{med,cool} = 1.7$ for cool plumes and $(L_p/L_{sz})_{med,warm} = 2.4$ for warm plumes.

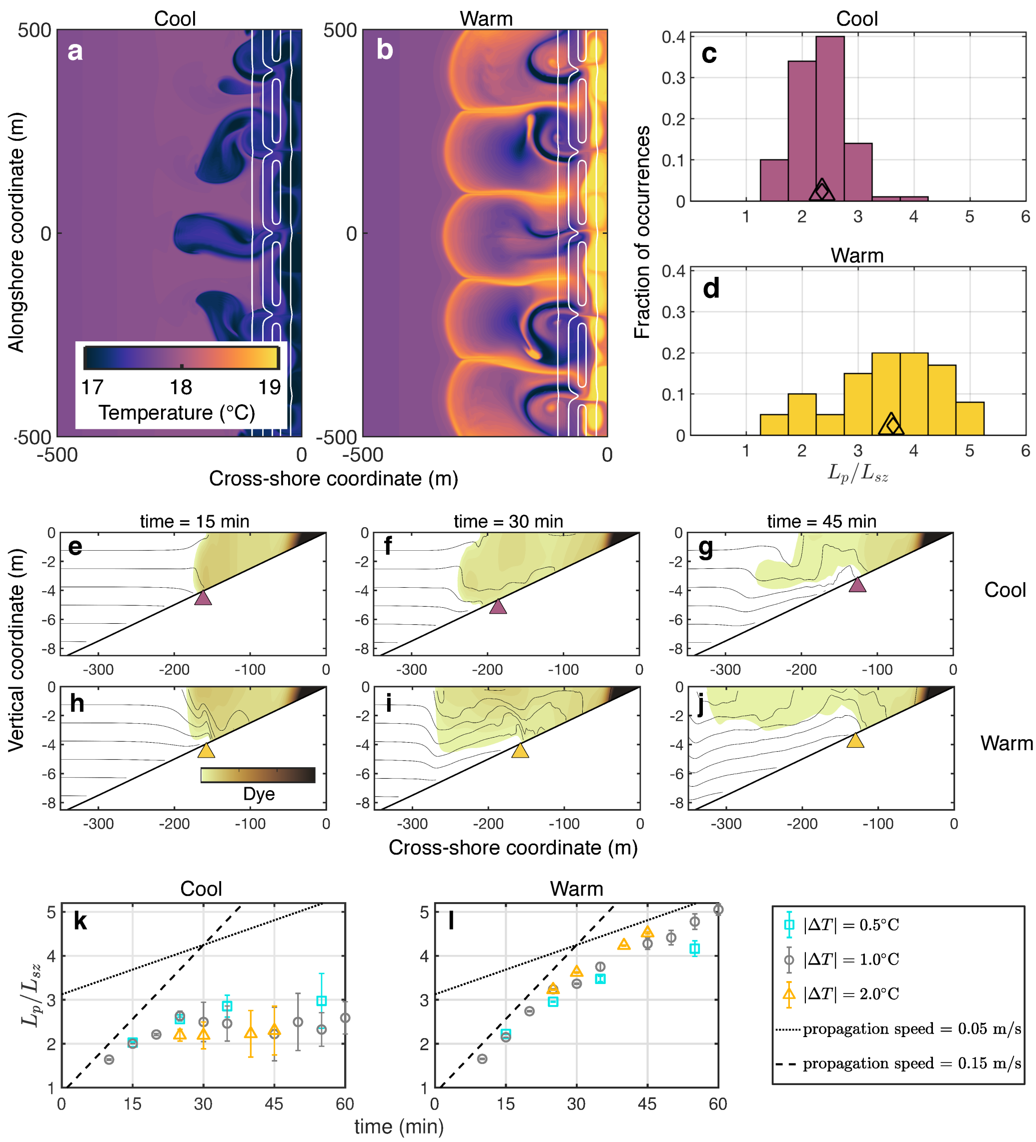

Figure 4. Surface temperature for modeled (a) cool and (b) and warm plumes with initial temperature difference between the surf zone and the shelf of $|\Delta T| = 1°C$ (Figure 2) at t=45 mins. Histograms of the fractional number of occurrences of (c) cool and (d) warm plumes in a suite of model simulations sampled at a range of times versus the normalized plume surface cross-shore extent (triangle: average, diamond: median). Cross-shore vertical sections of temperature (contours every 0.5°C) and the relative concentration of surfzone-released dye (color) through the center of a plume (y=200 m) for (e, f, g) cool or (h, i, j) warm plumes at t=15 min (e, h), t=30 min (f, i), and t=45 min (g, j). Triangles in (e-j) are locations where a baroclinic plume Froude number reaches unity, which approximately predicts plume liftoff. Temporal evolution of the mean (symbol) and standard deviation (vertical bars) of normalized plume surface cross-shore extent for (k) cool and (l) warm plumes for cases with $\Delta T = 0.5°C$ (cyan squares), 1°C (gray circles), and 2°C (orange triangles), with slopes of dotted and dashed lines indicating an expected range of gravity current propagation speeds.